

Late-Time *HST* Photometry of SN 1994I: Hints of Positron Annihilation Energy Deposition ¹

Alejandro Clocchiatti,² J. Craig Wheeler,³ Robert P. Kirshner,⁴ David Branch,⁵ Peter Challis,⁴ Roger A. Chevalier,⁶ Alexei V. Filippenko,⁷ Claes Fransson,⁸ Peter Garnavich,⁹ Bruno Leibundgut,¹⁰ Nino Panagia,¹¹ Mark M. Phillips,¹² Nicholas B. Suntzeff,¹³ Peter A. Höflich,¹⁴ and José Gallardo¹⁵

¹Based in part on observations with the NASA/ESA *Hubble Space Telescope*, obtained at the Space Telescope Science Institute, which is operated by the Association of Universities for Research in Astronomy (AURA), Inc., under NASA contract NAS 5-26555. This research is primarily associated with proposal GO–5777.

²Pontificia Universidad Católica de Chile, Departamento de Astronomía y Astrofísica, Casilla 306, Santiago 22, Chile; aclocchi@astro.puc.cl.

³Department of Astronomy, The University of Texas at Austin, Austin, TX, 78712; wheel@astro.as.utexas.edu.

⁴Harvard-Smithsonian Center for Astrophysics, 60 Garden Street, Cambridge, MA 02138; kirshner@cfa.harvard.edu, pchallis@cfa.harvard.edu.

⁵Homer L. Dodge Department of Physics and Astronomy, University of Oklahoma, 440 West Brooks, Room 100, Norman, OK 73019-2061; branch@phyast.nhn.ou.edu.

⁶Department of Astronomy, University of Virginia, P.O. Box 400325, Charlottesville, VA 22904-4325; rac5x@virginia.edu.

⁷Department of Astronomy, University of California, Berkeley, CA 94720-3411; alex@astro.berkeley.edu.

⁸Department of Astronomy, Stockholm University, AlbaNova, SE-10691 Stockholm, Sweden; fransson@astro.su.se.

⁹University of Notre Dame, Department of Physics, 225 Niewland Science Hall, Notre Dame, IN 46556-5670; pgarnavi@miranda.phys.nd.edu

¹⁰ESO, Karl-Schwarzschild-Strasse 2, Garching, D-85748, Germany; bleibund@eso.org.

¹¹Space Telescope Science Institute, 3700 San Martin Drive, Baltimore, MD 21218 (Also, Istituto Nazionale di Astrofisica [INAF], Rome, Italy, and Supernova Ltd., Virgin Gorda, British Virgin Islands); panagia@stsci.edu.

¹²Las Campanas Observatory, Casilla 601, La Serena, Chile; mmp@lco.cl.

¹³Texas A&M University, Physics Department, College Station, TX 77843;

Received _____; accepted _____

suntzeff@physics.tamu.edu.

¹⁴ Department of Physics, Florida State University, 315 Keen Building Tallahassee, FL 32306-4350; pah@physics.fsu.edu.

¹⁵ Centre de Recherche Astronomique, École Normale Supérieure de Lyon, France;jose.gallardo@ens-lyon.fr.

ABSTRACT

We present multicolor *Hubble Space Telescope* (*HST*) WFPC2 broadband observations of the Type Ic SN 1994I obtained ~ 280 d after maximum light. We measure the brightness of the SN and, relying on the detailed spectroscopic database of SN 1994I, we transform the ground-based photometry obtained at early times to the *HST* photometric system, deriving light curves for the WFPC2 *F439W*, *F555W*, *F675W*, and *F814W* passbands that extend from 7 d before to 280 d after maximum. We use the multicolor photometry to build a quasi-bolometric light curve of SN 1994I, and compare it with similarly constructed light curves of other supernovae. In doing so, we propose and test a scaling in energy and time that allows for a more meaningful comparison of the exponential tails of different events. Through comparison with models, we find that the late-time light curve of SN 1994I is consistent with that of spherically symmetric ejecta in homologous expansion, for which the ability to trap the γ -rays produced by the radioactive decay of ^{56}Co diminishes roughly as the inverse of time squared. We also find that by the time of the *HST* photometry, the light curve was significantly energized by the annihilation of positrons.

Subject headings: Supernovae

1. Introduction

Late-time light curves are an important piece of evidence for understanding supernova (SN) explosions. Conditioned by the always diminishing optical depth in the ejecta a time is always reached when the energy from radioactive decay is radiated on a time scale short compared with the dynamical time scale. Radiative equilibrium is established and there is a simple connection between energy produced, trapped, and radiated. The simplified physics permits a fairly direct connection between the light curve and the dynamical evolution of the expanding ejecta. This gives a more robust handle on some of the basic physical parameters of the explosion. How fast these late times are reached depend on the mass to energy ratio of the ejecta. For supernovae (SNe) without massive H envelopes they start a few weeks after maximum light.

The main physical processes at play are the emission of γ -rays and positrons from radioactive decays in the $^{56}\text{Ni} \rightarrow ^{56}\text{Co} \rightarrow ^{56}\text{Fe}$ chain (Colgate & McKee 1969), their interaction with the ejecta, and the spectrum of the radiation produced by the thermalization processes and the radiative transfer in the expanding ejecta. Some knowledge of the spectrum is important because ideal bolometric light curves are seldom observed, and astrophysicists generally must deal with observations that cover only a fraction of the radiated energy. The decay of ^{56}Ni into ^{56}Co releases energy in the form of γ -rays, with an e-folding time of 8.8 d, while the decay of ^{56}Co into ^{56}Fe releases $\sim 96\%$ of the energy in γ -rays and the remaining $\sim 4\%$ as positrons, with an e-folding time of 111.3 d (Diehl & Timmes 1998). Given a density structure and a chemical composition for the expanding ejecta, the γ -ray transport problem is determined. Positron interaction with the ejecta, on the other hand, strongly depends on the presence, and geometry, of magnetic fields (Ruiz-Lapuente & Spruit 1998). These are, and will probably remain, essentially free parameters. The escape of positrons from Type Ia supernovae (SNe Ia) may be relevant

to the diffuse 511 keV positron annihilation radiation from the Galactic bulge region (Knödlseeder et al. 2005).

Among SNe that explode through the gravitational collapse of the core, there are two distinct scenarios. For SNe II (see Filippenko 1997, for a review of SN types), associated with explosions of massive stars that have retained most of their H /He envelopes, and which are endowed with a relatively large mass-to-energy ratio, the ejecta are able first to trap the UV and optical-near IR photons for ~ 100 days, and then to trap the γ -rays from radioactive decays very efficiently for hundreds of days (e.g. Clocchiatti et al. 1996a; Elmhamdi et al. 2003). Since they trap essentially all of the energy from the radioactive decay of ^{56}Co during the time when both γ -rays and positrons are being produced, their light curves do not provide an effective diagnostic for the balance of γ -ray versus positron energy deposition. Something similar happens for many (though not necessarily all) Type Ib and Type IIb explosions.

SNe of Type Ic, on the other hand, associated with the explosion of stars that were massive while on the main sequence but that through individual and/or interactive binary evolution have lost all of the H and most of, if not all, the He of the outer layers, present more favorable conditions to study this problem. Their ejecta have a mass, and/or mass-to-energy ratio, small enough to allow a major fraction of the γ -rays from ^{56}Co to escape, potentially providing a cleaner window into the details of positron energy deposition.

The Type Ic SN 1994I in M51 presented a remarkable opportunity to build a useful late-time light curve for ejecta having both a low mass and a low mass-to-energy ratio. It exploded in a nearby galaxy and thus reached a bright apparent magnitude at maximum. Being in a host galaxy that is routinely observed by amateur astronomers meant, in addition, that the SN was spotted, reported, and spectroscopically confirmed well before maximum light (Puckett et al. 1994; Schmidt et al. 1994; Clocchiatti et al. 1994). Consequently, it

received extensive coverage both near maximum light and at later times.

An optical through near-infrared (IR) light curve extending ~ 50 d after maximum light was prepared by Schmidt (1994), and a more extensive one, reaching ~ 120 d after maximum, was presented by Richmond et al. (1996). The SN was, in addition, the target of many other programs, including radio and X-ray observations (Rupen et al. 1994a; Immler et al. 2002), and high-resolution spectroscopy of narrow absorption lines produced by significant amounts of foreground interstellar matter in M51 (Ho & Filippenko 1995). Extensive spectroscopic data sets were collected and presented by Filippenko et al. (1995) and Clocchiatti et al. (1996b). Finally, the light curve derived by Schmidt (1994) was the subject of detailed theoretical studies to set constraints on the physical parameters of the progenitor of SN 1994I and its evolutionary path to explosion (Nomoto et al. 1994; Iwamoto et al. 1994; Woosley et al. 1995).

In this paper, we present *Hubble Space Telescope (HST)* multi-wavelength broadband observations of SN 1994I, taken ~ 280 d after maximum light (~ 300 days after explosive nucleosynthesis). Combining these observations with those of Richmond et al. (1996), we build an optical through near-IR light curve that, via detailed modeling, can be used to set constraints on the ejected mass and its dynamical and thermal evolution. We introduce the new observations and photometry in § 2. In § 3 we describe the problems that need to be solved in order to combine the ground-based and space-borne observations, as well as the steps we took to construct our optical through near-IR light curve, and in § 4 we present the results. Our discussion in § 5 gives some physical interpretation based both on simplified models of the ejecta and γ -ray radiative transfer, and presents a revision and extension of the detailed model CO21 (Iwamoto et al. 1994). We summarize our conclusions in § 6.

2. Late-Time Observations and Photometry

The late-time data on SN 1994I were obtained with *HST* under the Supernova INTensive Studies (SINS) General Observer Program. On 1995 Jan. 15 (UT dates are used throughout this paper), about 280 d after maximum light, the WFPC2 on board *HST* was used to take five images of the SN in optical and near-IR passbands, totaling 3200 s of exposure time. The pointing of the telescope placed the SN on the Planetary Camera chip. Table 1 gives additional details of the observations. The images were reduced using the “On-The-Fly Reprocessing” pipeline, provided by the Space Telescope Science Institute (STScI).

Careful inspection of the images revealed the SN at the expected position, amidst the complex structure of one of the inner arms of M51. The right ascension and declination provided by the world coordinate system of the images was within 1'' of the position found by high-resolution radio interferometry with the Very Large Array (Rupen et al. 1994b). The identification was confirmed by analysis of two earlier sets of ultraviolet (UV) images also obtained with *HST*. They were obtained with WFPC2, when the SN was close to maximum light, using the *F336W* passband. One image, with an exposure time of 180 s, was taken on 1994 April 18, and a set of three images, with a combined exposure time of 1200 s, was obtained on 1994 May 12. The object identified as SN 1994I appears with very good signal in all images, and its flux diminishes by about a magnitude between the two epochs. A finder chart showing SN 1994I in the *HST* UV images is given in Figure 1, and stamps of the region around the SN in the UV, optical, and near-IR images are given in Figure 2.

The background against which the SN appeared is complex, but the exquisite resolution of PC1 placed the SN more than 15 pixels away from the closest source. The background light in the immediate vicinity of the SN appears to be relatively flat. Point spread function

(PSF) fitting photometry of the SN was done using HSTPhot (Dolphin 2000), which is calibrated with the zero points of Holtzman et al. (1995) by normalizing the PSF magnitude to aperture photometry with a $0.5''$ radius. The adopted version of HSTPhot had zero points and charge-transfer efficiency (CTE) correction parameters updated in 2002 October. The HSTPhot photometry of SN 1994I is given in Table 1.

3. Merging the Datasets and Estimating Extinction

If the late-time photometry of SN 1994I presented in the previous section is combined with the ground-based photometry of Richmond et al. (1996), the result will be a multicolor light curve extending from ~ 9 d before to ~ 280 d after maximum light. Very few SNe Ic have a multicolor light curve extending so long. Combining the datasets requires transforming the broadband observations between the different photometric systems used, and applying a correction for interstellar extinction.

The ground based observations of Richmond et al. (1996) were taken with three different combinations of instrument and telescopes but all of them referred to the standard system of Bessell (1990). We took the data from their Tables 4, 5, and 6, without making distinctions between datasets obtained with different telescopes, and selecting the dates for which all the B , V , R_C , and I_C bands had been observed. When more than one datapoint existed for the same day we combined them by a weighted average. This approach means that systematic differences in the calibration of the SN photometry due to the slightly different realizations of the standard system are interpreted as an uncertainty in the observation. The selected photometry is given in Table 2.

3.1. The Spectral Shape Corrections

Merging the space-borne and ground-based datasets calls for careful consideration of the passbands used. The differences in the SN flux measured by two different realizations of the same passband, evaluated in magnitudes, have been called “spectral shape corrections,” or S -corrections (Stritzinger et al. 2002; Krisciunas et al. 2004; Pignata et al. 2004). We generalize here the use of this name to the difference between the flux measured by a ground-based passband and its space-borne counterpart.

Computing the S -corrections requires precise knowledge of the passbands’ throughput and, ideally, spectra of SN 1994I at the specific dates of the photometry. The spectroscopic evolution of SN 1994I was closely followed (Filippenko et al. 1995; Clocchiatti et al. 1996b), although the last spectrum available was taken only ~ 147 d after maximum light, more than 130 d before the *HST* photometry. Regarding the passbands, those of the *HST* WFPC2 are well characterized¹, but three slightly different realizations of the ground-based $BV(RI)_C$ system were used by Richmond et al. (1996). Hence, as a model for the ground-based system, we computed the S -corrections as if the standard system were that of Bessell (1990), the one to which Richmond et al. (1996) attempted to transform. We estimated an uncertainty for these S -corrections by using different realizations of the Bessell passbands at assorted optical/near-IR imagers at the Cerro Tololo Interamerican Observatory and the Kitt Peak National Observatory. Note that we transformed the curves of Bessell (1990) from energy-based to photon-based units, and, for the other ground based passbands, we factored in a typical CCD quantum efficiency, the spectral response of two aluminum-coated surfaces, and the typical response of the sky telluric absorption bands if needed.

With this database of passbands and spectra, we explored whether it was better

¹See the URL <ftp://ftp.stsci.edu/cdbs> maintained by the STScI.

to transform the photometry from the space-borne to the ground-based system, or vice-versa. We found that because spectra are available at the times of the ground-based observations, it was preferable to convert the ground-based photometry to the space-based system. We computed S -corrections for the ground-based photometry using the spectra of Filippenko et al. (1995) and Clocchiatti et al. (1996b), and passbands as described above. We fit smooth polynomials to their time variation and used them to interpolate the S -correction and its uncertainty for the Richmond et al. (1996) observations. The results are included in Table 2.

3.2. Interstellar Extinction

All of the photometric and spectroscopic observations of SN 1994I indicate that it was heavily reddened by interstellar matter in M51. Different approaches to estimating A_V have included comparison with detailed theoretical models of light curves (Iwamoto et al. 1994) and spectra (Baron et al. 1996, 1999; Millard et al. 1999), and high-resolution spectroscopy of the narrow absorption lines produced by the gaseous phases of the interstellar matter (Ho & Filippenko 1995). Values of A_V from 0.9 up to 3.1 have been inferred, with a preferred range roughly between 1 and 2. We follow Richmond et al. (1996) in adopting $A_V = 1.4 \pm 0.5$ mag.

This value of A_V must next be translated into extinction for the different broadband filters. Typically an interstellar reddening law is adopted and scaled by the value of A_V , and the monochromatic fluxes obtained from the photometry are then corrected, applying the extinction value that the adopted law prescribes for the effective wavelength of the passbands. This approach, however, may lead to systematic errors when applied to objects with strong and variable emission lines. The effect is typically small, but it is systematic with time, tending to change the overall shape, and/or slope, of a light curve. Since the

extinction affecting SN 1994I is large, the issue merits consideration.

Again, the series of spectra of Filippenko et al. (1995) and Clocchiatti et al. (1996b) allow us to address this issue. Using these spectra, a typical interstellar extinction law (Cardelli, Clayton, & Mathis 1989), with $R_V = 3.1$, the transmittance of the passbands described earlier, and typical instrumental sensitivities, it is possible to compute the extinction affecting the spectra and its variation with time. The estimated extinction values and their uncertainties are included in Table 2.

The lack of a spectrum of SN 1994I some 280 d after maximum affects the estimates of interstellar extinction at the time, but the effect is small. Most of the variations that strongly affect the S -corrections at late times (changes of the emission lines in the near-IR) have a minor impact on the extinction.

We computed the extinction for the passbands of the *HST* WFPC2, fit smooth polynomials to the late-time trends, and extrapolated those from the latest observed spectrum out to the latest photometric point. To account for the uncertainty of the extrapolation, we increased the typical uncertainty of the fits by a factor of three for the last point. The extinction computed for the *HST* observation is included in Table 1.

The uncertainties due to the unknown details of the ground-based standard system realization and the lack of a very late-time spectrum are much smaller than the uncertainty of the overall extinction adopted ($\Delta A_V \approx 0.5$ mag according to Richmond et al. 1996). The changes in the light curves associated with the variation of the broadband extinction with time fall well within ΔA_V as well. However, computing the extinction from the evolving spectra and the expected passbands is the correct procedure for nonstellar spectra, and provides light curves that, for a given value of A_V , are free from the systematic effects related to the time variation of the extinction in each passband.

Two additional sources of uncertainty should be mentioned. First, the interstellar extinction law may not be the standard one. What can be said in this case is that, if the interstellar extinction towards SN 1994I follows the functional form of Cardelli, Clayton, & Mathis (1989) with a different value of R_V the difference will be smaller than the uncertainty in A_V , even for the more extreme values of R_V that they consider. Second, it is possible that at least a fraction of the extinction is produced in the local environment of the supernova. Since this local environment will be eventually affected by the evolution of the ejecta, a change of the foreground extinction with time would be conceivable. With the data available, it is not possible to set quantitative limits to this possibility.

4. The Light Curves

The resulting light curves of SN 1994I in the space-based system are shown in Figure 3, while the evolution of the photometric colors is given in Figure 4. The late-time point is consistent with the decrease in brightness and a flattening of the light curve expected from models that fit the post maximum decline (see below), and as suggested by the ground-based data earlier than ~ 80 d after maximum. The $(RI)_C$ magnitudes of the last two ground-based observations (at ~ 115 and ~ 140 d after maximum), and the B and V magnitude of the last ground-based observation, are not consistent with this trend. They appear to be slightly overluminous. The observed colors indicate little or no change of the overall spectral shape since the latest ground-based photometry.

With all the photometry transformed into the same system, it is possible to convert the observed single-bandpass light curves into monochromatic fluxes at the effective wavelengths, integrate them over wavelength, and obtain a new version of the “ $BV(RI)_C$ ”

light curve of SN 1994I². We used the zero points for the WFPC2 passbands given by Holtzman et al. (1995), and integrated the monochromatic fluxes using a simple trapezoid rule. We did not make any assumptions regarding the behavior of the flux beyond the limiting wavelengths of our coverage; flux beyond the limits of the B and I_C passbands was ignored. The distance of M51 was assumed to be 8.39 Mpc, based on the luminosity function of planetary nebulae (Feldmeier et al. 1997).

The $BV(RI)_C$ light curve of SN 1994I is shown in Figure 5, together with similarly constructed light curves of the Type Ic SNe 1990B (Clocchiatti et al. 2001), 1998bw (Patat et al. 2001; Sollerman et al. 2002; Clocchiatti et al. 2007), and 2002ap (Tomita et al. 2006). The latter two have been modeled with ejecta of low mass-to-energy ratio (Iwamoto et al. 1998; Mazzali et al. 2002), but fairly large ejected mass, and have also sometimes been called “hypernovae.” As a benchmark of absolute brightness and evolution timescales, the $BV(RI)_C$ light curve of the normal Type Ia SN 1992A (N. Suntzeff, 2006, private communication) is also given.

5. Discussion

5.1. Simple Comparisons

The light curves in Fig. 5 illustrate the wide range that SNe Ic span in absolute brightness, and show that the diversity cuts across observational borders proposed to classify them, like the supernova or hypernova categories. Fig. 5 also shows that SN 1994I was fairly luminous reaching more than 50% of the brightness of normal Type Ia SN. A

²Even though it was calibrated using the space-borne WFPC2 passbands, we prefer to name the light curve using the more compact designation of their equivalent ground-based passbands.

foreground extinction a few tenths of a magnitude larger, which is consistent with model light curves, spectra, or high-resolution spectra of the narrow Na D absorption lines, would make it as bright as SN 1992A. The $BV(RI)_C$ light curves also confirm that, similar to the behavior close to maximum light, the time scale for brightness variation of SN 1994I at late times was fast. The early exponential tail of SN 1994I is faster than that of the other Type Ic SNe, and comparable to that of the Type Ia SN.

Qualitative comparison with the late-time light curves of SNe 1990B, 1998bw, and 2002ap indicates a mismatch between the trend suggested by the last ground-based photometric points and the HST observation. SN 1994I shows a sharp downward change of slope in the exponential tail after ~ 140 days, not seen in the other SNe Ic. The rate of decay measured from the data between ~ 80 and ~ 140 d after explosion is 43% slower than that measured using the points between ~ 40 and ~ 80 d, and the change happens very fast, between 80 and 115 d after explosion. By contrast, the decline slope of SN 1990B is essentially constant at these times, that of SN 1998bw changes by less than $\sim 28\%$ between earlier than 80 d after explosion and later than 250 d after explosion, and that of SN 2002ap changes by $\sim 7\%$ in this same time period.

If the trend suggested by the last two ground-based photometric points were correct, then something fairly dramatic happens to the $BV(RI)_C$ light curve between ~ 140 and ~ 300 d after maximum light. One possibility is the so-called “infrared catastrophe” that shifts energy from the optical/near-IR passbands into the far-IR (Fransson & Chevalier 1989; Kozma & Fransson 1998), though it is not expected at such relatively early epochs in SNe Ic. Another possibility is that the brightness at 300 days after maximum is affected by a different amount of foreground local extinction, as it would happen if the ejecta of SN 1994I formed dust. This is, however, not consistent with the small, or nill, change in broadband colors.

Another possibility is that the latest ground based photometric points are affected by contamination from background light from M51. Richmond et al. (1996) did image matching and subtraction before performing photometry, but the background of SN 1994I was particularly bright and had a steep gradient over the spatial scales sampled by the PSF of the ground-based images. Thus, residual contamination in the ground-based images could be present.

5.2. Comparison with a Simple Model

When γ -ray radiative transfer can be approximated by a pure absorption process (Sutherland & Wheeler 1984), the radioactive nickel assumed to be located at the center of the ejecta, accounting for a small fraction of the total mass (i.e. a point source model for the γ -ray emission), and the SN ejecta modeled by a spherically symmetric distribution of matter in free expansion, the optical depth that extinguishes the γ -rays decreases with the inverse of time squared (e.g. Clocchiatti & Wheeler 1997). In this case, the energy deposited by γ -rays can be approximated by

$$E_{\gamma} \propto \exp(-t/\tau_{\text{Ni}}) \{1 - \exp[-(T_0/t)^2]\}, \quad (1)$$

where τ_{Ni} is the e-folding time for the decay of ^{56}Co , and T_0 is the characteristic time for a given ejecta structure, which depends on its mass M , energy E , density profile, and the absorption cross section per unit mass (κ) that matter presents to γ -rays. For a given density profile, $T_0 \propto (\kappa M^2/E)^{1/2}$. Soon after maximum light, when radiative equilibrium is established, the above assumptions are expected to hold. Then, in addition, between 100% and $\sim 96\%$ of the radioactive energy is released in γ -rays, and most of them are trapped in the ejecta. In these conditions, E_{γ} gives a good representation of the energy available to heat the ejecta and equation 1 can be fitted to bolometric light curves to estimate the parameter T_0 . At later times, as the fraction of γ -rays that escape from the ejecta increases,

the $\sim 4\%$ of energy released in the form of positrons needs to be considered. In what follows, we will consider the two extreme possibilities for thermalization of the positron annihilation energy: either they are completely trapped in the ejecta, or they escape.

Assuming that the $BV(RI)_C$ light curve of SN 1994I, between ~ 40 and ~ 80 d after explosion, is a good representation of the bolometric light curve, we fit the light curve to determine $T_0 \approx 65$ d, if the energy from the ^{56}Co positrons is completely deposited, or $T_0 \approx 67$ d, if the positrons escape from the ejecta without interacting. The $BV(RI)_C$ luminosity with these fitted simple models is shown in Figure 6.

The simple models are very good at fitting the data between ~ 40 and ~ 80 d after explosion, suggesting some connection with reality, and they do a reasonably good job at ~ 300 d. Since the (bolometric) model implies $\sim 50\%$ more energy than the $BV(RI)_C$ observation, the data taken at face value would be consistent either with full trapping of positrons from ^{56}Co and a small bolometric correction at ~ 300 d, or with a smaller (even null) bolometric correction and a more complex process of positron transfer that traps $\sim 50\%$ of their total energy. It should be noted, though, that the simple model without positron trapping falls below the observed light curve. The simplest interpretation of this observation is that SN 1994I did trap a significant fraction of the positrons.

The last two points from ground-based photometry (between ~ 100 and ~ 120 days after explosion) are missed by both fits. We note, in addition, that it is not possible to obtain a good fit for the simple models of eq. 1 when all the ground-based observations of the exponential tail (between ~ 40 and ~ 120 d after explosion) are included, even if the *HST* point at 300 d is excluded. The problem is the fast change in the slope of the $BV(RI)_C$ light curve between ~ 80 and ~ 115 d after explosion. Fitting this break requires including an additional free parameter, like two different values of T_0 , which could represent a model of two different mass components each of them with different expansion properties.

As a comparison, it is possible to successfully fit eq. 1 to the exponential decay of the light curves of all the other SNe Ic shown in Fig. 5³.

5.3. Simple Comparison with Hindsight From the Simple Model

In §5.1 we compared the derived light curves of several SNe. Although it is illustrative to see how different SN light curves behave in a plot like that of Fig. 5, it is not completely correct to compare the evolution of different ejecta on a calendar-time basis. What we would like to do is to plot the light curves using units that are more physically meaningful.

From a few tens to a few hundreds of days after explosive nucleosynthesis, the evolution of the bolometric light curves is governed by two main time scales: τ_{Co} , the e-folding time for the radioactive decay of ^{56}Co into ^{56}Fe , and T_0 , the characteristic time for the decrease of the γ -ray optical depth (eq. 1). They are, respectively, the time scale for energy production and the time scale for energy deposition. This suggests that the natural *energy* scale to compare late-time light curves of different SNe is $L_{\text{Bol}}(t_n)/\exp(-t_n/\tau_{\text{Co}})$, where t_n is measured since nucleosynthesis, and that the natural scale to compare the time evolution of the ejecta is t_e/T_0 , where t_e should be measured from the start of free expansion. Since, at the times of interest, the difference between t_n and t_e is negligible, either of them may be used. We fitted the models of eq. 1 to the light curves of all SNe Ic in Fig. 5, and then normalized the energy and time axes according to the previous prescription. The result is shown in Figure 7.

It is reassuring to confirm that such a simple scaling brings some “order” to Fig. 5. When the energy is normalized by the input ^{56}Co source, and time by the natural scale for

³We note also that eq. 1 fails to provide a good fit to the late-time light curve of the Type Ia SN 1992A.

γ -ray deposition (responsible for most of the energy available to the ejecta from soon after maximum until the supply of ^{56}Co is exhausted), all of the late-time light curves follow approximately the same track. It is possible to bring them into close agreement just by normalizing the total amount of ^{56}Ni ejected by the explosion (i.e. the additive constant in the logarithm of the energy used in Fig. 5).

This comparison shows that, in units of the natural time scale of evolution of the γ -ray optical depth, the late-time point of SN 1994I presented in this paper (~ 280 d after maximum) is even more extreme than those observed for SN 1998bw and SN 2002ap, which had light curves extending beyond ~ 500 d after maximum. Also, it shows that, in comparison with Eq. 1, the three very late light curves are consistent with a flattening after $\sim 3T_0$, a time at which the γ -ray optical depth becomes negligible, and most of the γ -rays escape into space. For SN 1994I, the exact time at which the flattening occurs is unknown due to the lack of observations. However, both at $3T_0 \approx 200$ d, and at 300 d corresponding to the last observation, a modest fraction of ^{56}Co remains in the ejecta, and the $\sim 4\%$ of the radiated energy that its decay releases in the positron channel becomes a significant source.

Regarding the late-time ground-based photometry, the scaling of Fig. 7 confirms the arguments given before. The last two points depart from the common locus, and probably overestimate the luminosity of SN 1994I due to background contamination.

5.4. Insights From a Detailed Model

Iwamoto et al. (1994) presented a model of SN 1994I which, without fine tuning of the structure, provides a good fit to the early part of the $UBV(RI)_C$ light curve, from ~ 6 d before up to ~ 40 d after maximum light. Their preferred configuration is a C+O core that would result from the evolution of a massive star in an interacting binary system that

underwent two mass-transfer episodes. Depending on the initial parameters of the binary, at the moment of explosion the pair consists of the presupernova and a neutron star, white dwarf, or low-mass main-sequence companion (Nomoto et al. 1994).

Iwamoto et al. (1994) fitted the light curves of SN 1994I provided by Schmidt (1994) with the explosion of a star that entered the main sequence with $\sim 15M_{\odot}$, became a $\sim 4.0M_{\odot}$ He star after the first mass transfer, and a $2.1 M_{\odot}$ C+O core after the second (model CO21). A simultaneous fit of the monochromatic and $UBV(RI)_C$ curves required an interstellar reddening of $E(B - V) = 0.45$ mag, and a distance of 6.92 Mpc ($m - M = 29.2$ mag), in good agreement with the values used to determine the $BV(RI)_C$ light curve presented here.

Would model CO21 fit the very late-time *HST* photometry? The question is relevant because previous attempts at fitting SN light curves over long time spans have uncovered a problem. When the models are good at fitting the maximum light they tend to be too dim on the tail; conversely, if they are good at fitting the late-time decay, they tend to give a maximum broader and/or brighter than observed. Solving this problem has typically meant introducing free parameters in the density structure of the model (Ensman & Woosley 1988; Tomita et al. 2006).

Based on the explosion model CO21 (Iwamoto et al. 1994), and using the same radiative transfer code, we calculated the monochromatic light curves, but here we extend the computations to 300 days after explosion. The assumptions and approximations used in the code are described in more detail in (Iwamoto et al. 1994) and (Höflich, Müller & Khokhlov 1993). A hypothesis relevant to our discussion below, is that all positrons are thermalized locally and cannot escape. Because of the limitations of the code in the treatment of forbidden lines and their time dependence, we assumed the energy distribution to be unchanged after day 120. This assumption is consistent with the observations because the

color indices scarcely change after about 100 d (Table 2 and Fig. 4). The assumption prevents us from testing overall migration of flux toward the IR, as may result from the formation of dust. The evolution of the colors, however, suggest that neither dust formation, nor other change in the foreground extinction by matter in the circumstellar region, do occur in this SN.

From the monochromatic fluxes, we calculated the magnitudes in each relevant *HST* passband. We checked that the synthetic *F439W* and *F555W* values agree with the *B* and *V* of Iwamoto et al. (1994) within a few hundredths of a magnitude. The small differences can be attributed to adjustments in the frequency grid and differences in the *HST* filter functions and the Bessell system, since *S*-corrections were not applied in this test.

From the monochromatic fluxes at the effective wavelength of the passbands, we built a $BV(RI)_C$ light curve using the same procedure as in the observations (see §4). We compare the theoretical light curves of model CO21 with the observations in Fig. 6. Both the bolometric and $BV(RI)_C$ luminosities are plotted. They are very similar, indicating that the model concentrates most of the energy within the passbands observed. Overall, the model luminosities agree well with the observations, especially in the post-maximum decay, although some details merit further comment.

At maximum, the model results dimmer than the observations, while the same model fits better the $UBV(RI)_C$ in Iwamoto et al. (1994). One reason for that is the distance. The observed $BV(RI)_C$ light curve presented here is based on an observed distance of 8.39 Mpc (Feldmeier et al. 1997), while, for the same foreground extinction, CO21 is consistent with a distance 1.47 Mpc shorter in Iwamoto et al. (1994). The shorter distance will help our model $BV(RI)_C$ light curve to fit the maximum better, but will give a brighter than required post maximum decay. This highlights the importance of using extensive datasets when comparing models to observations.

The $BV(RI)_C$ light curve of CO21 shown in Fig. 6 does fit most of the observed $BV(RI)_C$ light curve of SN 1994I. First, the distance independent width of the observed maximum, and then the distance dependent brightness of the post-maximum decline and exponential decay. Fitting the peak-to-tail contrast will require some additional fine tuning.

A possible hint is that the model $UBV(RI)_C$ light curve does a better job at fitting the peak-to-tail contrast of the $BV(RI)_C$ observations, indicating that the model spectrum overestimates the fraction of total flux emerging in the ultraviolet at early times. In any case, the problem of CO21 is opposite to the traditional peak-to-tail contrast problem: if the maximum of the $BV(RI)_C$ model is arbitrarily shifted to match the observed one, then the model light curve results brighter than the observed, not dimmer. Studying the peak-to-tail contrast problem in SN light curves is beyond the scope of this paper, so we will let the issue rest there.

The late-time tail of the detailed model, which includes a realistic approximation to the γ -ray transfer and deposition, follows closely the simple deposition function given by eq. 1, with full trapping of the positrons from the decay of ^{56}Co . Since CO21 also assumes full trapping of positrons, this is an indication that the γ -ray transfer is well represented by the simple approximations that went into eq. 1. Hence, the conclusion stated above that about half of the positrons are able to deposit their energy within the ejecta is supported by the more elaborate model as well.

6. Conclusions

Through the *HST* GO SINS program, we observed SN 1994 with WFPC2 when the SN was about 280 d past maximum light. We did PSF photometry on the resulting images

using HSTPhot (Dolphin 2000).

We collected published ground-based photometry of SN 1994I, applied a reddening correction, and transformed the results to the space-based HST WFPC2 photometric system. Both the reddening correction and the photometric transformation were based on the extensive spectroscopic database available for the SN (Filippenko et al. 1995; Clocchiatti et al. 1996b). The resulting light curves in the $F439W$, $F555W$, $F675W$, and $F814W$ passbands span from ~ 7 d before to ~ 280 d after maximum light.

Using the zero points and effective wavelengths of Holtzman et al. (1995), we transformed the multicolor photometry to monochromatic flux, and then integrated the flux over the available wavelength range to construct a “ $BV(RI)_C$ ” light curve. We compared the $BV(RI)_C$ light curve of SN 1994I with those of other SNe Ic, and, based on a simplified model of the ejecta, proposed a scaling in energy and time that provides a more insightful comparison of the exponential tails of different SNe. The light curves that reach times larger than $\sim 3T_0$, where T_0 is the characteristic time for the decay of the γ -ray optical depth, show a clear flattening. For rapidly evolving SNe, like SN 1994I, a simple interpretation of this flattening is that the small percentage of energy that the decay of ^{56}Co releases in the form of positrons becomes a relevant thermal energy source for the ejecta.

Model CO21, originally presented by Iwamoto et al. (1994), does a reasonable job at fitting both the $BV(RI)_C$ and monochromatic light curves at early times. We extended the original light-curve calculations up to day 300. We note that the absolute $BV(RI)_C$ luminosity agrees well with the observations of SN 1994I up to about 80 d after maximum light, but overestimates the flux by $\sim 50\%$ at day 300.

Models with full positron trapping indicate that some energy was missed by the observations, but models without positron trapping indicate an observed excess of energy. The missing (or excess) energy amounts to $\sim 50\%$ of that produced by the annihilation

of ^{56}Co positrons. Although models with no positron trapping *and* a migration of energy toward the mid-to-far IR (e.g., by dust formation) cannot be ruled out, a simpler interpretation of these late-time observations is that the ejecta of SN 1994I trapped $\sim 50\%$ of the positrons roughly 300 d after the explosion.

Our interpretation of the $BV(RI)_C$ light curve is consistent with the SN evolving as a freely expanding envelope whose optical depth to γ -rays decreases, very approximately, with the inverse of time squared. Simple models that treat the deposition of γ -rays as a pure absorption process, and the more detailed model CO21, agree on this. SN 1994I does not need a model with two dynamically distinct components, like the one that Tomita et al. (2006) propose for SN 2002ap.

We conclude that our very late-time $BV(RI)_C$ photometry represents most of the energy that the SN produced at this time, implying that the late-time bolometric correction of this rapidly evolving SN Ic was not large. This, in turn, would mean that the “infrared catastrophe” in this SN does not happen until phases later than ~ 300 d.

Although model CO21 was not finely tuned to closely match the observed light curves of SN 1994I, it helps to show that the late-time photometry presented here is extreme in terms of the γ -ray optical depth, and agrees with the simple models of eq. 1 in that the dominant source of late-time energy originates in positrons. A model built specifically to represent this SN could be used to establish a meaningful constraint on the fraction of positrons actually trapped in the ejecta, and whether (and when) there is a migration of photons from the optical and near-IR to the IR region of the spectrum.

A.C. thanks the Department of Astronomy of the University of Texas at Austin for support from a W. M. Cox Visitor Grant and from the Samuel T. and Fern Yanagisawa Regents Professorship in Astronomy, and acknowledges the support of CONICYT, Chile,

under grants FONDECYT 1051061 and FONDAP 15010003. The *HST* SINS program was supported by NASA through grants GO–2563 and GO–5777 from the Space Telescope Science Institute, which is operated by the Association of Universities for Research in Astronomy (AURA), Inc., under NASA contract NAS 5–26555. J.C.W. was supported in part by NASA Grant NNG04GL00G and NSF Grant AST–0406740. A.V.F. is grateful for the support of NSF grant AST–0607485. This research made use of the SUSPECT online database of SN spectra (<http://bruford.nhn.ou.edu/~suspect/>).

REFERENCES

- Baron, E., Branch, D., Hauschildt, P. H., Filippenko, A. V., & Kirshner, R. P., 1999, ApJ, 527, 739
- Baron, E., Hauschildt, P. H., Branch, D., Kirshner, R. P., & Filippenko, A. V., 1996, MNRAS, 279, 799
- Bessell, M., 1990, PASP, 102, 1181
- Cardelli, J. A., Clayton, G. C., & Mathis, J. S. 1989, ApJ, 345, 245
- Clocchiatti, A., Brotherton, M., Harkness, R. P., Wheeler, J. C., Mikuz, H., & Corwin, H. 1994, IAU Circ., 5972, 2
- Clocchiatti, A., et al., 1996, AJ, 111, 1286
- Clocchiatti, A., & Wheeler, J.C., 1997, ApJ, 491, 375
- Clocchiatti, A., Wheeler, J. C., Brotherton, M. S., Cochran, A. L., Wills, D., Barker, E. S., & Turatto, M. 1996, ApJ, 462, 462
- Clocchiatti, A., et al., 2001, ApJ, 553, 886
- Clocchiatti, A., et al., 2007, in preparation
- Colgate, S. A., & McKee, C., 1969, ApJ, 157, 623
- Diehl, Roland; Timmes, F. X.
- Diehl, R., & Timmes, F. X., 1998, PASP, 110, 637
- Dolphin, A. E. 2000, PASP, 112 1397
- Elmhamdi, A., Chugai, N. N., & Danziger, I. J. 2003, A&A, 404, 1077

- Ensmann, L. M., & Woosley, S. E. 1988, *ApJ*, 333, 754
- Feldmeier, J., Ciardullo, R., & Jacoby, G. 1997, *ApJ*, 479, 231
- Filippenko, A., et al., 1995, *ApJ*, 450, L11
- Filippenko, A. V. 1997, *ARA&A*, 35, 309
- Fransson, C., & Chevalier, R. A. 1989, *ApJ*, 343, 323
- Ho, L. C., & Filippenko, A. V. 1995, *ApJ*, 444, 165 “[Erratum: 1996, 463, 818]”
- Höflich, P., Müller, E., Khokhlov, A. M. 1993, *A&A*268, 570
- Holtzman, J.A. et al. 1995, *PASP*, 107, 1065
- Immler, S., Wilson, A. S., & Terashima, Y. 2002, *ApJ*, 573, L27
- Iwamoto, K., Nomoto, K., Höflich, P., Yamaoka, H., Kumagai, S., & Shigeyama, T. 1994, *ApJ*, 437, L115
- Iwamoto, K., et al., 1998, *Nature*, 395, 672
- Knödseder, J., et al. 2005, *A&A*, 441, 513
- Kozma, C., & Fransson, C., 1998, *ApJ*, 496, 946
- Krisciunas, K., et al. 2004, *AJ*, 127, 1664
- Mazzali, P. A., et al. 2002, *ApJ*, 572, L61
- Millard, J., et al., 1999, *ApJ*, 527, 746
- Nomoto, K., Yamaoka, H., Pols, O. R., van den Heuvel, E. P. J., Iwamoto, K., Kumagai, S., & Shigeyama, T. 1994, *Nature*, 371, 227

- Patat, F., et al. 2001, *ApJ*, 555, 900
- Pignata, G., et al. 2004, *MNRAS*, 355, 178
- Puckett, T., et al. 1994, *IAU Circ.*, 5961, 1
- Richmond, M. W., et al. 1996, *AJ*, 111, 327
- Ruiz-Lapuente, P., & Spruit, H. C., 1998, *ApJ*, 500, 360
- Rupen, M. P., Sramek, R. A., Weiler, K., Panagia, N., & Van Dyk, S. 1994a, *Bulletin of the American Astronomical Society*, 26, 1361
- Rupen, M. P., Sramek, R. A., Weiler, K., Van Dyk, S., & Panagia, N. 1994b, *IAU Circ.*, 5963
- Schmidt, B., 1994, private communication
- Schmidt, B., Kirshner, R., Peters, J., & Bernstein, G. 1994, *IAU Circ.*, 5962, 2
- Sollerman, J. et al. 2002, *A&A*, 386, 944
- Stritzinger, M., et al. 2002, *AJ*, 124, 2100
- Sutherland, P., & Wheeler, J. C. 1984, *ApJ*, 280, 282
- Tomita, H., et al. 2006, *ApJ*, 644, 400
- Woosley, S. E., Langer, N., & Weaver, T. A. 1995, *ApJ*, 448, 315

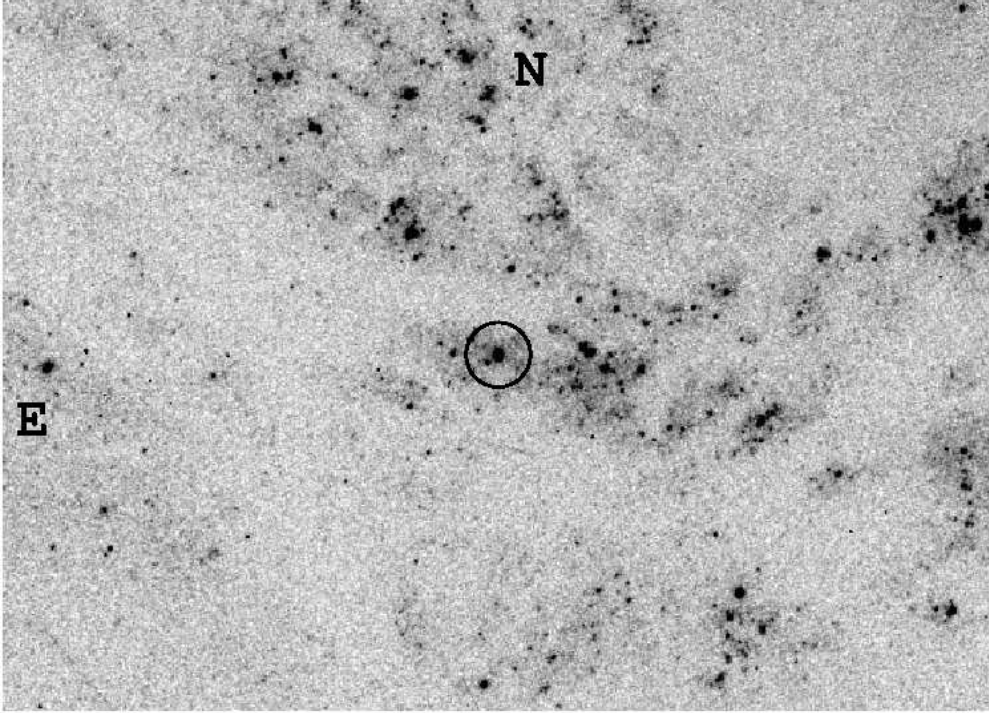


Fig. 1.— *HST* image of SN 1994I and its surroundings. The SN is at the center of the frame, inside the circle. North is at the top and East is to the left. The width of the field displayed is about $28''$. The image shown is the combination of the three images taken on 1994 May 12, with the *F336W* passband.

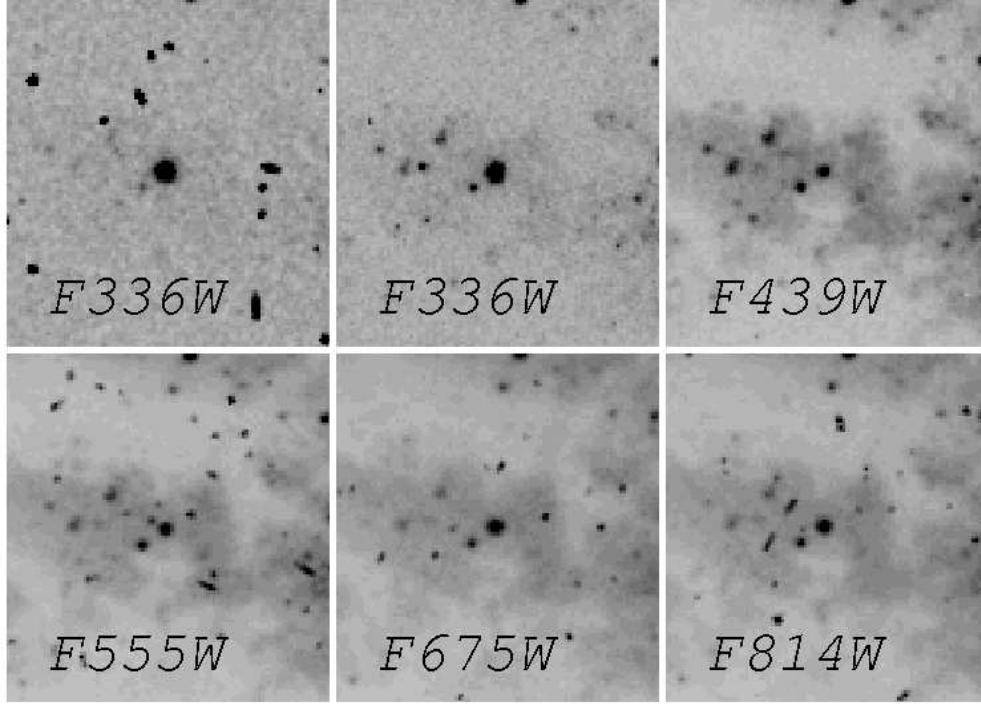


Fig. 2.— Stamps of the region around SN 1994I in the *HST* images. North is at the top, and East is to the left. The width of each stamp is $4.6''$. The passbands used are indicated by labels. SN 1994I is at the center of each stamp. The top-left stamp corresponds to the *F336W* exposure taken on 1994 April 18, while the top-center stamp is an expanded view of the 1994 May 12 image shown in Figure 1. The dimming of SN 1994I in the 24 elapsed days is clear. The other images were taken on 1995 Jan. 15 (see Table 1).

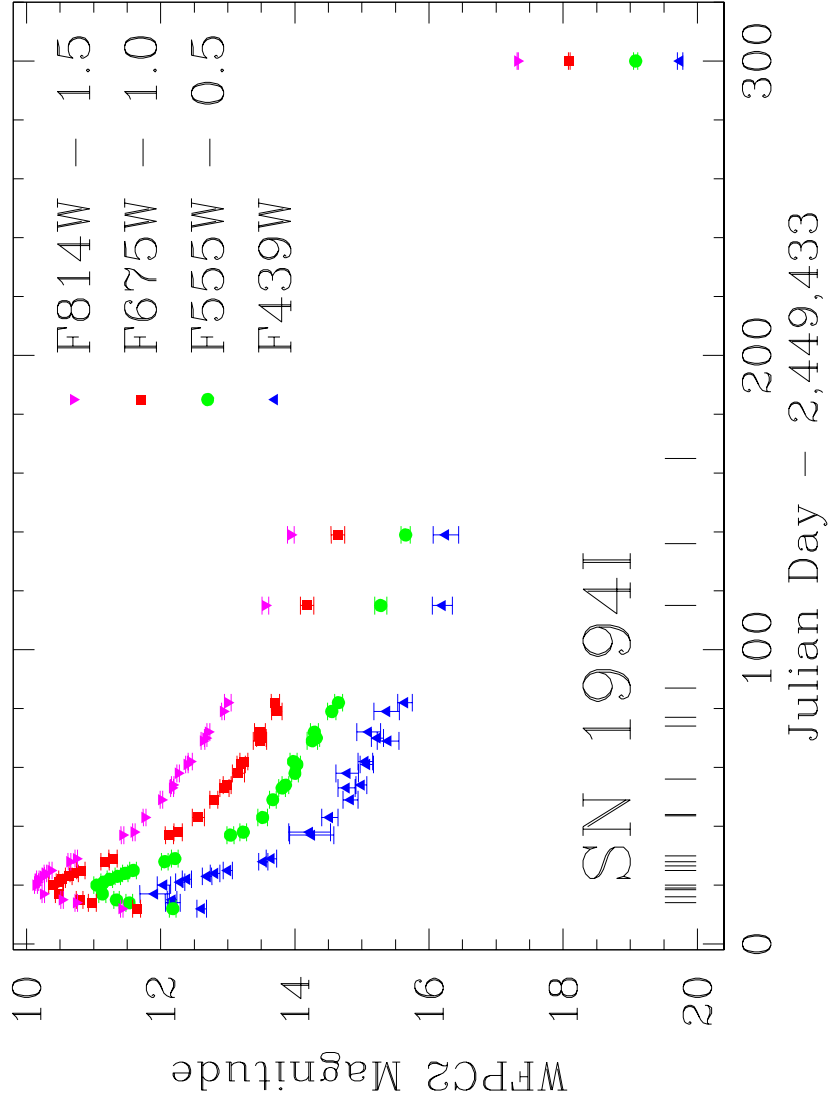


Fig. 3.— *HST* WFPC2 broadband unreddened photometry of SN 1994I (the last point, at $JD - 2,449,433 \approx 300$), and ground-based B , V , R_C , and I_C photometry (Richmond et al. 1996) unreddened and translated to the WFPC2 passbands. The vertical marks above the lower horizontal axis indicate the times at which the spectra of Filippenko et al. (1995) and Clocchiatti et al. (1996b) were taken. The shift in time corresponds to the explosion date ($JD = 2,449,433$) estimated by Iwamoto et al. (1994).

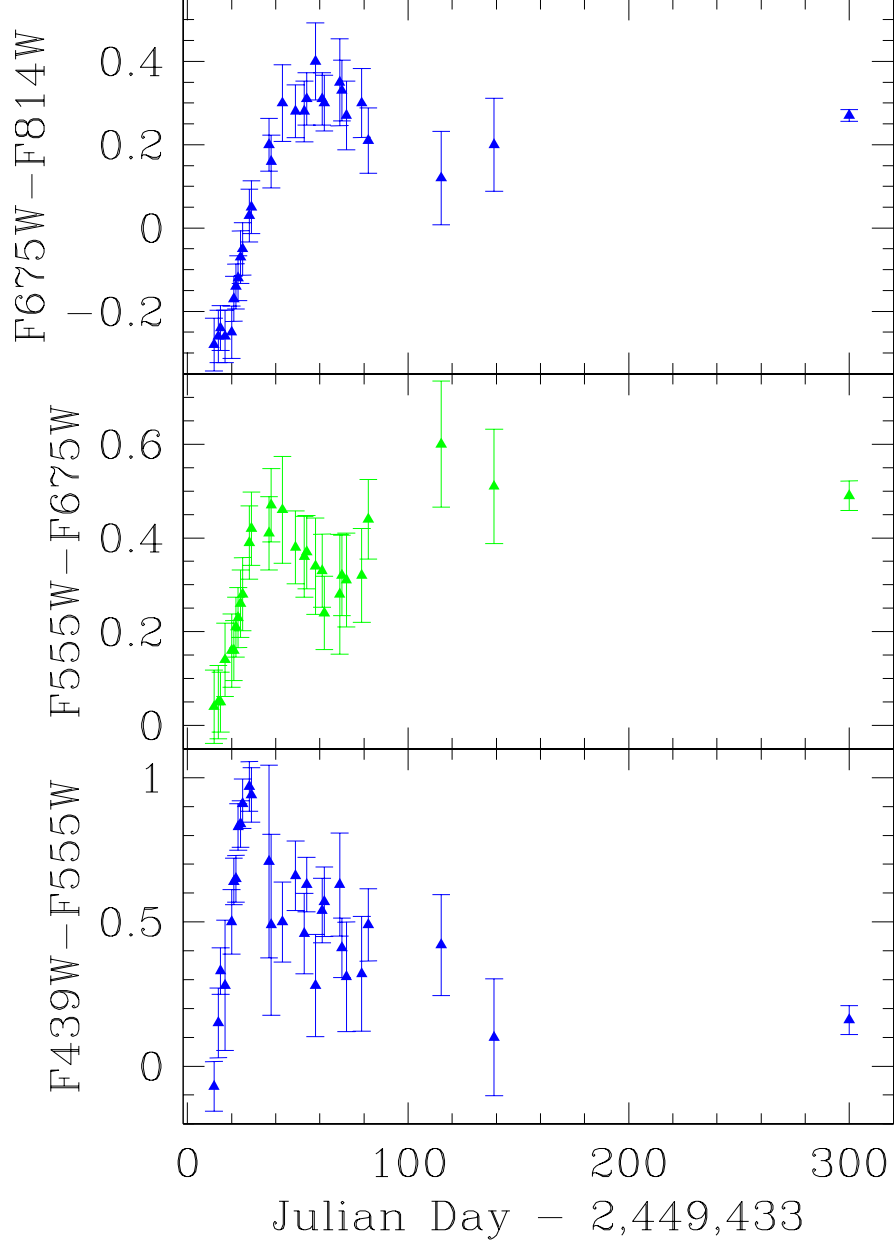


Fig. 4.— *HST* WFPC2 broadband unreddened colors of SN 1994I in the HST passbands computed from the photometry of Figure 3. The shift in time corresponds to the explosion date ($JD = 2,449,433$) estimated by Iwamoto et al. (1994).

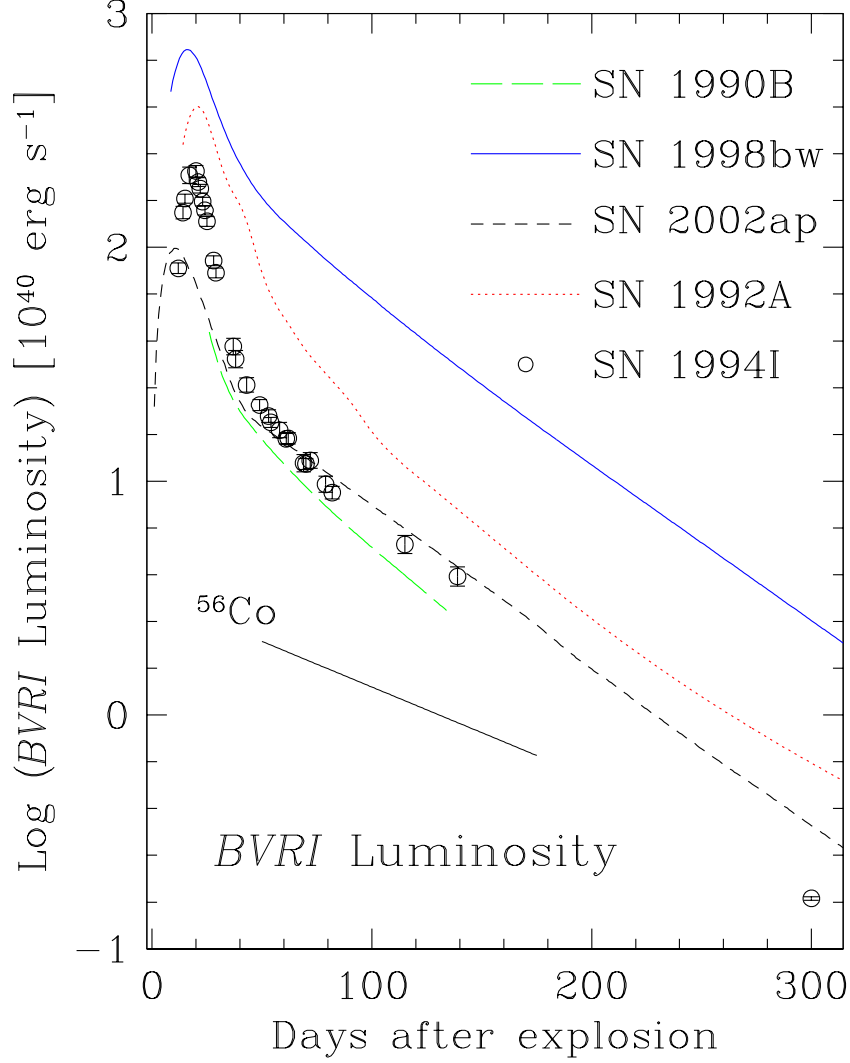


Fig. 5.— $BV(RI)_C$ light curves of the Type Ic SNe 1994I, 1990B, 1998bw, and 2002ap, as well as of the Type Ia SN 1992A. The light curve of SN 1990B has been displaced downward by 0.5 vertical units for clarity. Explosion-date estimates are from a theoretical light-curve fit for SN 1994I (Iwamoto et al. 1994), theoretical spectra and light-curve fits for SN 2002ap (Mazzali et al. 2002), and the date of GRB 980425 for SN 1998bw. For SN 1990B the explosion date was taken from Clocchiatti et al. (2001), who estimated it from comparison with SN 1993J, and for SN 1992A the explosion date was assumed to be ~ 20 d before maximum light in B . The slope for full trapping of the ^{56}Co decay products is also shown.

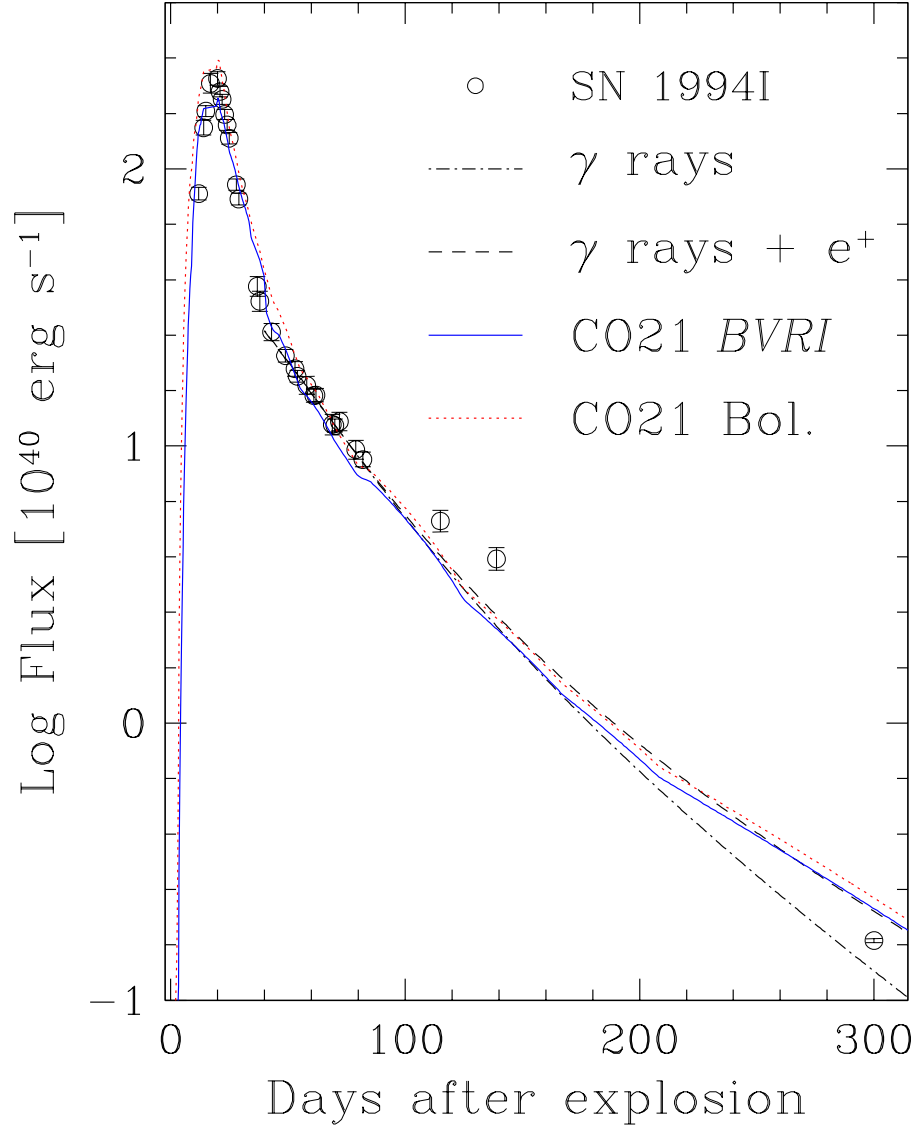


Fig. 6.— $BV(RI)_C$ light curve of SN 1994I, the simple models given by eq. 1, and model CO21.

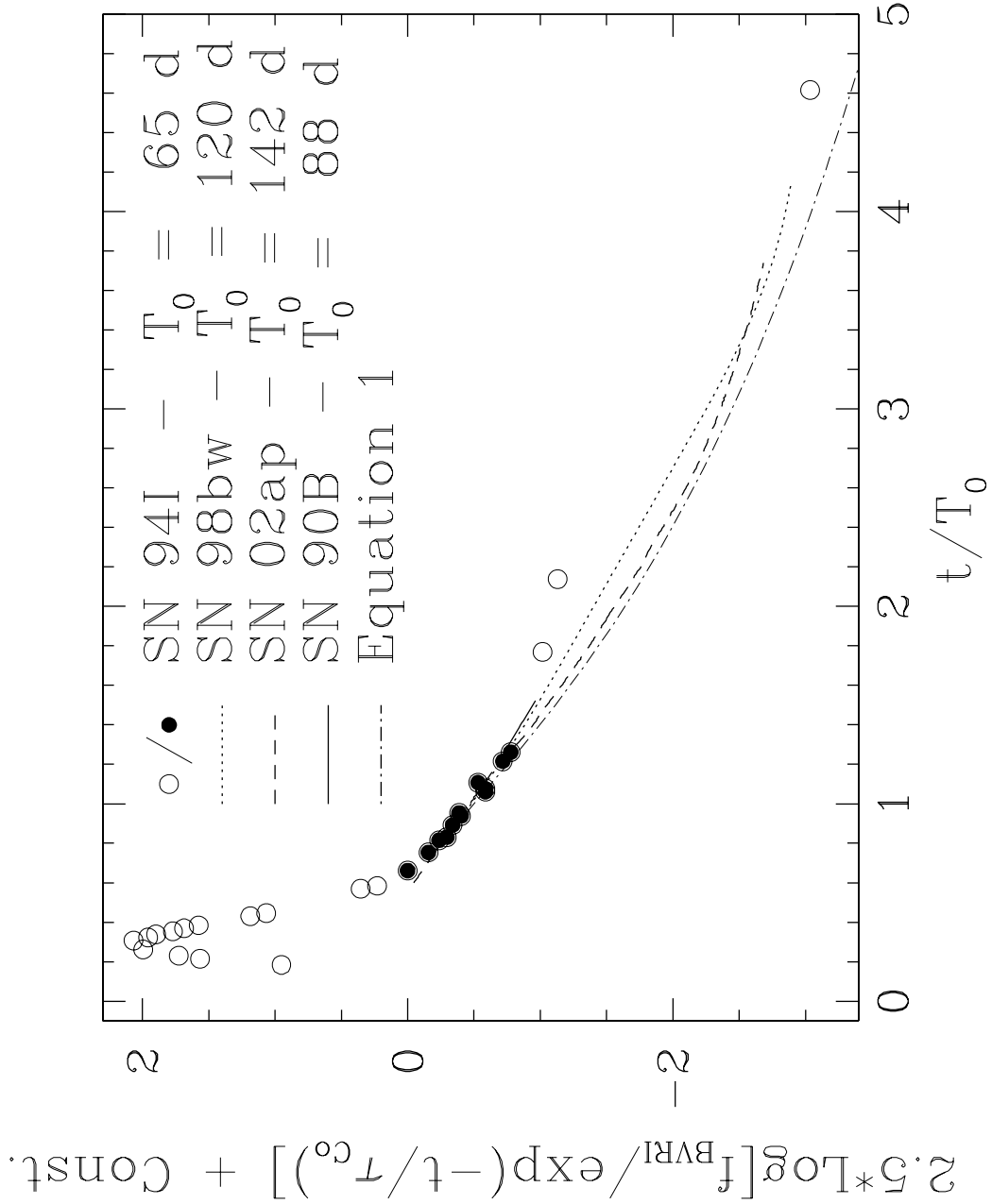


Fig. 7.— $BV(RI)_C$ late-time light curves of SNe Ic 1994I, 1998bw, 2002ap, and 1990B, normalized according to the prescriptions of § 5.3. Points mark the observations of SN 1994I. Solid symbols indicate the region used to fit the time-scale parameter T_0 . A constant was added to the light curves of SNe 1994I, 1998bw, 2002ap, and 1990B, to make them match the solid points of SN 1994I.

Table 1. Late-Time *HST* Photometry of SN 1994I

<i>HST</i> Dataset	JD ^a	Exp. ^b	Passband	<i>HST</i> Mag.	Extinction ^c
U2LQ0201T/2T	733.21	1400	<i>F439W</i>	21.63 ± 0.02	1.89 ± 0.033
U2LQ0203T	733.22	600	<i>F555W</i>	21.03 ± 0.01	1.45 ± 0.030
U2LQ0204T	733.25	600	<i>F675W</i>	20.21 ± 0.01	1.12 ± 0.010
U2LQ0205T	733.26	600	<i>F814W</i>	19.69 ± 0.01	0.87 ± 0.010

^aMean Julian Date of total exposure minus 2,449,000. For phase, subtract an additional 433.00.

^bTotal exposure time in the passband (in seconds). Two *F439W* exposures of 700 s each were combined in one image.

^cInterstellar extinction in the host galaxy, in the *HST* passband.

Table 2. Ground-Based Photometry of SN 1994I

JD ^a	B^b	V^b	R_C^b	I_C^b	A_B^c	A_V^c	$A_{R_C}^c$	$A_{I_C}^c$	SC_B^d	SC_V^d	$SC_{R_C}^d$	$SC_{I_C}^d$
445	14.41 ± 0.03	14.04 ± 0.02	13.87 ± 0.02	13.77 ± 0.01	1.83	1.40	1.17	0.86	-0.03	-0.04	0.05	-0.01
447	13.97 ± 0.08	13.39 ± 0.02	13.21 ± 0.02	13.09 ± 0.02	1.83	1.40	1.17	0.86	-0.04	-0.04	0.06	-0.01
448	13.95 ± 0.02	13.20 ± 0.01	13.02 ± 0.01	12.88 ± 0.01	1.83	1.40	1.17	0.86	-0.05	-0.04	0.06	-0.01
450	13.68 ± 0.21	12.99 ± 0.02	12.72 ± 0.02	12.60 ± 0.02	1.83	1.40	1.17	0.86	-0.06	-0.04	0.06	0.00
453	13.81 ± 0.07	12.91 ± 0.02	12.62 ± 0.02	12.49 ± 0.02	1.83	1.40	1.17	0.86	-0.07	-0.04	0.06	0.00
454	14.05 ± 0.02	13.02 ± 0.01	12.72 ± 0.01	12.52 ± 0.01	1.83	1.40	1.17	0.86	-0.07	-0.04	0.06	0.00
455	14.15 ± 0.02	13.11 ± 0.01	12.76 ± 0.01	12.53 ± 0.01	1.83	1.40	1.17	0.86	-0.08	-0.04	0.06	0.00
456	14.44 ± 0.01	13.23 ± 0.01	12.86 ± 0.01	12.61 ± 0.01	1.83	1.40	1.17	0.86	-0.08	-0.04	0.06	0.00
457	14.56 ± 0.02	13.34 ± 0.01	12.94 ± 0.02	12.64 ± 0.01	1.83	1.40	1.17	0.86	-0.08	-0.04	0.06	0.00
458	14.75 ± 0.02	13.46 ± 0.02	13.04 ± 0.02	12.72 ± 0.02	1.83	1.41	1.17	0.86	-0.08	-0.04	0.06	0.00
461	15.28 ± 0.03	13.93 ± 0.02	13.41 ± 0.02	13.00 ± 0.02	1.83	1.41	1.17	0.86	-0.09	-0.04	0.06	0.00
462	15.40 ± 0.04	14.08 ± 0.02	13.53 ± 0.03	13.10 ± 0.02	1.83	1.41	1.17	0.85	-0.09	-0.03	0.06	0.00
470	16.00 ± 0.32	14.92 ± 0.02	14.37 ± 0.03	13.79 ± 0.01	1.84	1.41	1.17	0.85	-0.09	-0.03	0.07	0.01
471	15.97 ± 0.30	15.11 ± 0.02	14.50 ± 0.02	13.96 ± 0.02	1.84	1.41	1.17	0.85	-0.09	-0.03	0.07	0.01
476	16.28 ± 0.10	15.41 ± 0.05	14.80 ± 0.07	14.12 ± 0.01	1.84	1.41	1.17	0.85	-0.08	-0.02	0.07	0.01

Table 2—Continued

JD ^a	B^b	V^b	R_C^b	I_C^b	A_B^c	A_V^c	$A_{R_C}^c$	$A_{I_C}^c$	SC_B^d	SC_V^d	$SC_{R_C}^d$	$SC_{I_C}^d$
482	16.61 ± 0.08	15.56 ± 0.02	15.03 ± 0.03	14.37 ± 0.02	1.84	1.41	1.17	0.85	-0.06	-0.02	0.07	0.01
486	16.56 ± 0.11	15.71 ± 0.03	15.20 ± 0.04	14.53 ± 0.01	1.84	1.41	1.17	0.85	-0.05	-0.01	0.08	0.01
487	16.78 ± 0.04	15.76 ± 0.02	15.24 ± 0.03	14.54 ± 0.02	1.84	1.41	1.17	0.85	-0.05	-0.01	0.08	0.01
491	16.58 ± 0.16	15.90 ± 0.03	15.41 ± 0.07	14.62 ± 0.02	1.84	1.41	1.17	0.85	-0.04	-0.01	0.08	0.01
494	16.88 ± 0.07	15.94 ± 0.02	15.45 ± 0.03	14.75 ± 0.02	1.84	1.41	1.17	0.85	-0.03	-0.01	0.08	0.02
495	16.86 ± 0.09	15.89 ± 0.02	15.49 ± 0.02	14.80 ± 0.03	1.84	1.41	1.17	0.85	-0.03	-0.01	0.08	0.02
502	17.21 ± 0.14	16.18 ± 0.07	15.73 ± 0.09	15.00 ± 0.03	1.84	1.41	1.17	0.85	-0.02	0.00	0.08	0.02
503	17.06 ± 0.06	16.24 ± 0.02	15.75 ± 0.04	15.04 ± 0.02	1.84	1.41	1.17	0.85	-0.02	0.00	0.08	0.02
505	16.93 ± 0.17	16.21 ± 0.04	15.74 ± 0.06	15.08 ± 0.02	1.84	1.41	1.17	0.85	-0.01	0.00	0.09	0.02
512	17.21 ± 0.18	16.48 ± 0.04	15.99 ± 0.06	15.30 ± 0.02	1.84	1.42	1.17	0.85	-0.01	0.01	0.09	0.02
515	17.48 ± 0.08	16.58 ± 0.04	15.97 ± 0.03	15.37 ± 0.05	1.84	1.42	1.17	0.85	0.00	0.01	0.09	0.02
548	18.05 ± 0.13	17.23 ± 0.08	16.46 ± 0.08	15.95 ± 0.05	1.85	1.42	1.17	0.86	0.00	0.03	0.11	0.03
572	18.10 ± 0.18	17.60 ± 0.06	16.93 ± 0.09	16.34 ± 0.05	1.85	1.42	1.17	0.86	0.00	0.04	0.12	0.04

^aMean Julian Date minus 2,449,000. For phase, subtract an additional 433.00.

^bPhotometry from Tables 4, 5, or 6 of Richmond et al. (1996).

^cInterstellar extinction in the host galaxy, in the given ground-based passband. Mean uncertainties (mag) are $\delta A_B = 0.060$, $\delta A_V = 0.010$, $\delta A_{Rc} = 0.003$, and $\delta A_{Ic} = 0.003$.

^d S -correction to be subtracted from the ground-based magnitude to transform to the space-borne equivalent passband (see Table 1). Mean uncertainties (mag) are $\delta SC_B = 0.033$, $\delta SC_B = 0.041$, $\delta SC_{Rc} = 0.053$, and $\delta SC_{Ic} = 0.014$.